ACI STRUCTURAL JOURNAL TECHNICAL PAPER

Title No. 118-S99

Shear Behavior of Concrete Walls Retrofitted with Ultra-High-Performance Fiber-Reinforced Concrete Jackets

by Renaud Franssen, Luc Courard, and Boyan I. Mihaylov

Ultra-high-performance fiber-reinforced concrete (UHPFRC) possesses outstanding mechanical properties and high durability, and thus can provide effective retrofit solutions for concrete walls and wall-type bridge piers. This self-leveling material can be cast in thin layers around the pier to protect it from corrosive environments and to enhance its shear resistance. However, while this is a promising solution, research has focused mostly on the retrofit of slabs and beams. To address this gap in knowledge, this paper presents results from four large-scale tests of shear-critical concrete walls with and without UHPFRC jackets. The test variables are the thickness of the jacket, the preparation of the concrete surface, and the level of axial load. It is shown that water-jetting of the surface ensures an effective composite action of the concrete and UHPFRC, while a smooth surface results in early debonding. It is also demonstrated that, while the reference reinforced concrete specimen failed in brittle shear, water-jetted walls with 30 and 50 mm jackets reached their flexural capacity and exhibited enhanced crack control. In addition to test results, the study also proposes and validates a three-degree-of-freedom kinematic model to accurately describe the deformation patterns of UHPFRC-strengthened walls.

Keywords: kinematic model; retrofit; shear; ultra-high-performance fiber-reinforced concrete (UHPFRC); wall-type bridge piers; walls.

INTRODUCTION

The maintenance of large aging infrastructure across the world poses serious technical, environmental, and economic challenges. In many countries, a large number of bridges suffer from serious degrees of corrosion, while the resources for their rehabilitation are limited. Corrosion in concrete bridges typically occurs due to carbonation, chloride ion ingress, or sulfate reaction in the most exposed zones of the bridge; refer to Fig. 1(a). To rehabilitate these zones in a sustainable and cost-effective manner, a solution using a new generation of materials—ultra-high performance fiber-reinforced concretes (UHPFRC) with compressive strength of up to 250 MPa—has emerged in the past 20 years.[2] UHPFRC materials are characterized by outstanding mechanical properties as well as high durability due to their extremely low permeability.[3,4] As shown in Fig. 1(b),[1] this self-leveling material can be cast in thin layers on the deck and around the bridge piers to protect the structure from corrosive environment, and in this way to significantly extend its service life. In addition, the UHPFRC layers can be used to increase the stiffness and strength of the structure, which is often required due to material degradation, increased traffic loads, construction/design errors or damage due to accidental loads.

This paper focuses on the UHPFRC rehabilitation and strengthening of walls and wall-type bridge piers, and in particular the most corroded zones of the pier immediately above the foundations; refer to Fig. 1(b). The corrosion reduces the section of the horizontal shear reinforcement which is the closest to the surface of the member. In such situations, jackets of UHPFRC cast around the bridge pier can both stop the corrosion process and strengthen the pier against brittle shear failures. The strengthening effect is mainly due to the enhanced tension behavior of UHPFRC characterized by high tensile strength (7 to 15 MPa versus approximately 2 MPa for regular concrete), effective crack control, and significant ductility.[5,6]

However, while UHPFRC jackets can provide an effective retrofit solution for bridge piers, research has focused mostly on the rehabilitation and strengthening of slabs and beams.[2,7,8] In such members, the addition of a layer of UHPFRC on the flexural tension side of the section has been shown to significantly increase the stiffness, delay cracking, and enhance both the flexural and shear strength.[9,10] In beams, U-shaped UHPFRC jackets have been used successfully to suppress brittle shear failures and to ensure a flexure-dominated ultimate behavior.[11] Nevertheless, there are limited experimental studies confirming the technological feasibility of thin vertical UHPFRC layers[12-16] and, to the authors' knowledge, no tests have focused on the shear resistance of UHPFRC-retrofitted wall-type piers. Therefore, this paper is aimed at addressing these knowledge gaps and facilitating the use of UHPFRC for the retrofit of bridges piers. The paper reports the results from four large-scale tests of shear-critical concrete walls with and without UHPFRC jackets. The study also lays the basis for a rational kinematics-based theory capable of capturing the effect of UHPFRC jackets on the shear behavior of retrofitted walls.

RESEARCH SIGNIFICANCE

While UHPFRC retrofit of structures has been studied in the past 20 years, most of the research has focused on the behavior of bridge deck slabs and slender beams, while very few researchers have studied the behavior of UHPFRC-jacketed wall-type members. To help close this gap in knowledge, this study reports detailed results of an experimental

ACI Structural Journal, V. 118, No. 5, September 2021.

MS No. S-2020-273.R1, doi: 10.14359/51732825, received February 12, 2021, and reviewed under Institute publication policies.

(a) Bridge piers with advanced corrosion (photos courtesy of Service Public de Wallonie)

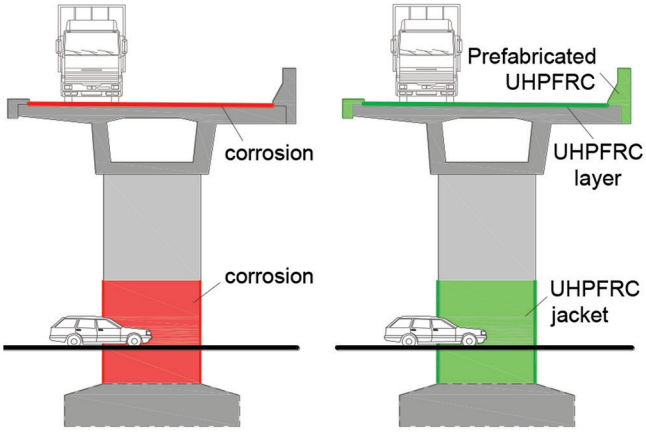

(b) UHPFRC retrofitting of concrete bridges (adapted from Brühwiler[1])

Fig. 1—Corrosion and retrofit of concrete bridges (adapted from Brühwiler[1]).

campaign on four large-scale shear walls reinforced with UHPFRC jackets, as well as a kinematic model to analyze the deformation behavior of the walls.

EXPERIMENTAL PROGRAM

Test specimens

The experimental program consisted of testing to failure of four nominally identical concrete walls with a 230 x 1500 mm rectangular section (Fig. 2). The clear height of the walls was 2300 mm and the height subjected to shear was $a = 2550$ mm, resulting in an aspect ratio $a/h = 2550/1500 = 1.7$. One of the walls was a reference reinforced concrete member, while the other three were retrofitted with UHPFRC jackets covering the bottom 1500 mm of the member. The jackets were cast after removing a layer of surface concrete all around the section. The thickness of the jackets was the same as that of the removed concrete, and therefore the retrofitted walls had the same cross-sectional dimensions as the reference specimen. The walls were fixed in a concrete foundation block, while the load on the walls was applied via a top concrete block.

The two main tests variables were the thickness of the UHPFRC jacket and the preparation of the interface between the concrete and UHPFRC. The reference specimen RF0 had no jacket, specimens RF30s and RF30r had 30 mm thick

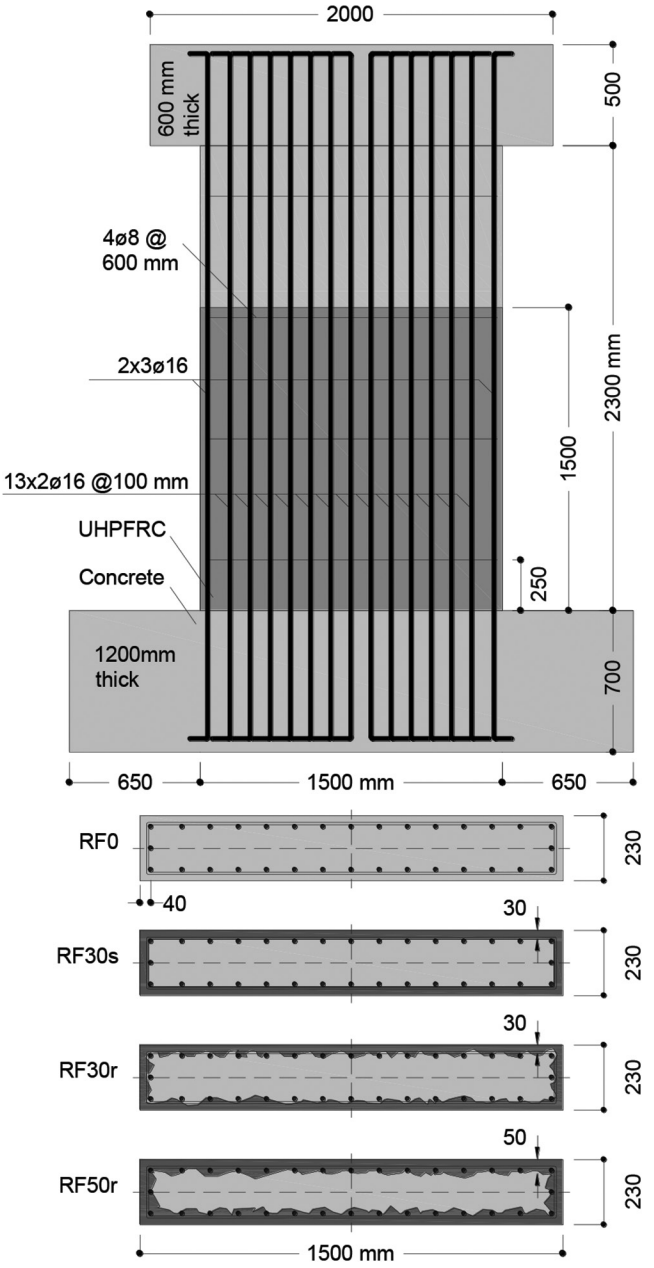

Fig. 2—Test specimens.

jackets, and RF50r had a 50 mm thick jacket. The concrete of specimens RF30r and RF50r was removed by water-jetting, resulting in a rough surface. In contrast, specimen RF30s was cast with a smooth "negative" formwork (refer to section Construction of Tests Specimens for details), and thus featured a smooth interface. This latter test was used to simulate a limit situation of a poor surface preparation with a low resistance to interface shear.

The longitudinal reinforcement of the walls consisted of ϕ16 bars distributed uniformly across the section (Fig. 2). The bars were anchored in the top and bottom concrete blocks without lap splicing, and their total area was 1.87% of the gross concrete area of the section. To represent existing bridge piers with corroded shear reinforcement, the specimens had only four ϕ8 stirrups with a stirrup ratio of 0.073%. The stirrups were anchored with 90-degree hooks to simulate poor detailing in existing structures. The top and bottom

concrete blocks of the specimens were heavily reinforced to avoid significant deformations in these regions.

Materials

The four walls were designed to have the same concrete with a compressive strength f_c' of approximately 50 MPa and a maximum aggregate size of 16 mm. The actual strength of each specimen was determined as the average from three 160 x 320 mm concrete cylinders tested on the day of the wall test. Table 1 summarizes the age and strengths of the concrete and UHPFRC, as well as the mechanical properties of the reinforcing bars.

The UHPFRC used for the jackets was a commercial product provided by the company WELL. It had a cement matrix with a maximum aggregate size of 2 mm, as well as straight steel fibers with a diameter of 0.2 mm and a length of 17 mm. The tensile strength of the fibers was 2200 MPa and the fiber volumetric ratio was 1.25%.

A series of tests were performed to characterize the UHPFRC. Cylinder tests on 110 x 220 mm specimens were conducted similarly to those for the concrete, resulting in an average compressive strength $f_c'_{UHPFRC}$ of 123 MPa (Table 1). In addition to strength, these tests were also used to measure the modulus of elasticity E_{UHPFRC} and pre-peak stress-strain response in compression as illustrated in Fig. 3(a). The tensile response of the UHPFRC was determined from bending tests of 100 x 100 x 400 mm prisms in accordance with the French design recommendations.[17,18] Four-point bending tests without a notch were used to determine the modulus of rupture reported in Table 1, while three-point tests with a 10 mm notch were used to obtain the crack width versus tensile stress response in Fig. 3(b). An inverse analysis was used to calculate the curves in Fig. 3(b) from the crack width versus load response measured in the tests.[17,18] It can be seen from Fig. 3(b) and Table 1 that the peak tensile resistance of the UHPFRC exceeded the modulus of rupture (approximately 6.5 MPa versus 5.4 MPa), and therefore the material exhibited a slight tension-hardening behavior. According to the French design recommendations, the average fiber orientation factor in the prisms is estimated at 0.52. However, direct measurements in other studies[19-22] have shown that if the prism casting is performed from one side as in this study, this factor can reach values as high as 0.86.

Construction of tests specimens

The concrete wall specimens were cast in two stages—the bottom block first, and the test region and top block second—without special roughening of the concrete in the construction joints. For Specimen RF30s, the section in the bottom 1500 mm of the wall was reduced by attaching 30 mm thick expanded polystyrene sheets to the inner face of the formwork (negative formwork) (Fig. 4(a)). After the specimens were cured, the surface concrete of specimens RF30r and RF50r was removed by a water-jetting robot that produced a significant surface roughness (Fig. 4(b)). In Specimen RF30r the rough surface was on average aligned with the external face of the longitudinal reinforcement, while in RF50r the water-jetting penetrated behind the reinforcement.

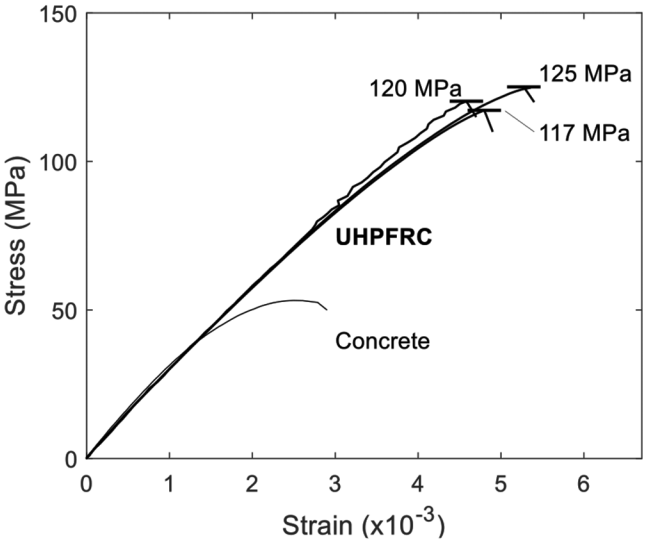

(a) Compressive behavior of concrete and UHPFRC

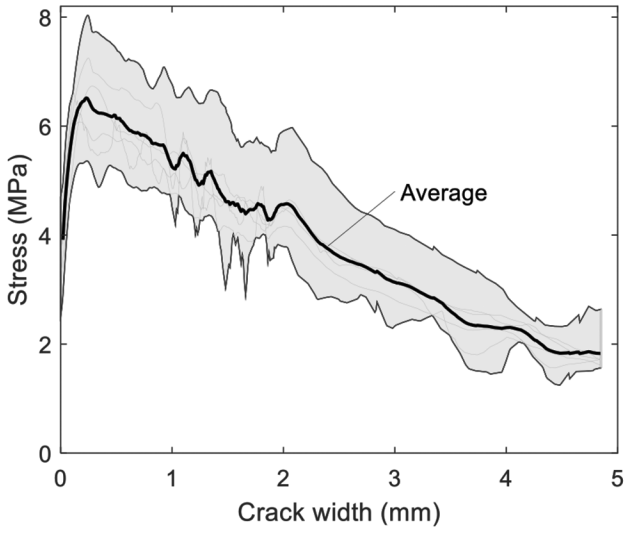

(b) Tensile behavior of UHPFRC

Fig. 3—Measured behavior of concrete and UHPFRC.

To build the UHPFRC jackets, a formwork was installed around walls RF30s, RF30r, and RF50r, and the concrete surface was wetted lightly. The UHPFRC was cast with a bucket through two openings with shoots at the top of the formwork (Fig. 4(c)). After the removal of the formwork, a gap varying from 0 to 100 mm was observed at the top of the jackets of walls RF30r and RF50r, and a subsequent cast was needed to fill the gap. Wall RF30s did not have a gap as a consequence of problems with its formwork that bulged out during the casting. To recover the original geometry, the formwork was clamped externally using steel sections and prestressing rods. This operation put pressure on the liquid UHPFRC and resulted in the complete filling of the formwork. In practice, gaps at the top of the jacket can be avoided by using taller shoots that create additional pressure on the UHPFRC during casting.

Table 1—Measured material properties

Wall	RF0	RF30s	RF30r	RF50r
Concrete age, days	147	181	201	243
f_c', MPa	52.3	52.6	46.4	45.5
E_c, GPa	35.0	33.4	34.2	33.9
UHPFRC age, days	—	71	104	146
$f_{c'UHPFRC}$, MPa	—	119.5	124.5	126.2
E_{UHPFRC}, GPa	—	28.7	28.9	29.0
Rupture modulus, MPa	—	5.4	5.4	5.4
Peak tensile resistance, MPa	—	6.5	6.5	6.5
f_y ϕ16 (ϕ8), MPa	522 (577)			
f_u ϕ16 (ϕ8), MPa	609 (638)			
ε_u ϕ16 (ϕ8), %	7.00 (5.20)			

Note: f_c' and $f_{c'UHPFRC}$ are compressive strength of concrete and UHPFRC, respectively; E_c and E_{UHPFRC} are modulus of elasticity of concrete and UHPFRC; f_y and f_u are yield strength and tensile strength of reinforcement; ε_u is rupture strain of reinforcement.

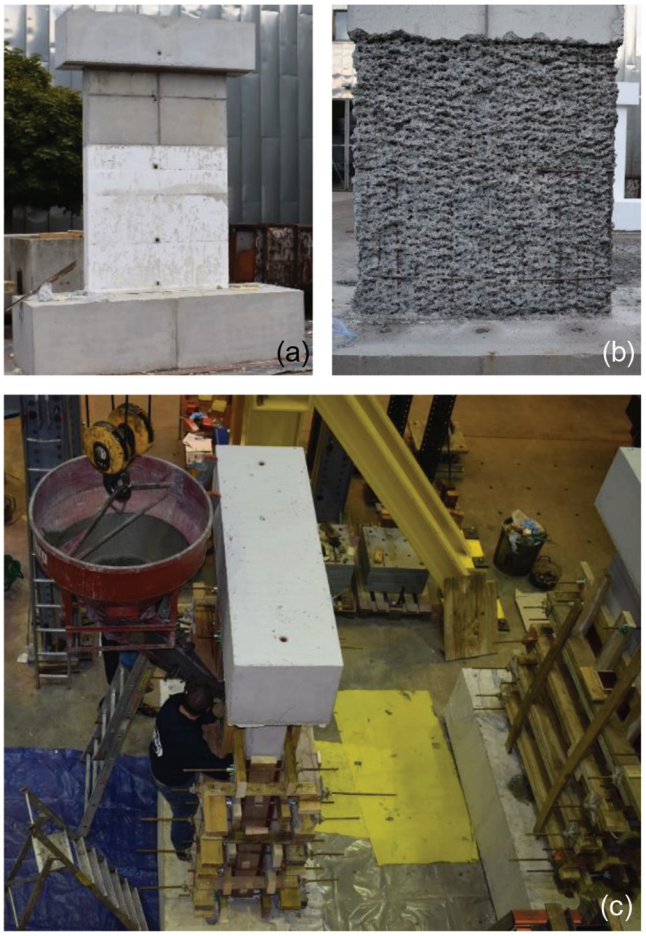

Fig. 4—Construction of test specimens.

Loading procedure and instrumentation

Figure 5 shows the test setup used for the loading of the walls in the structural laboratory at the University of Liège. The bottom block of the specimens was post-tensioned to the strong floor to prevent uplift and sliding during loading. To simulate gravity loads, a concentric vertical load was applied on the top block via a still assembly and six high-strength steel bars, three on each side of the specimen. The bars were stressed from underneath the strong floor by using hydraulic jacks. Walls RF0, RF30s, and RF30r were loaded with an axial compression force N = 1200 kN ($n = N/bhf_c'$ = ~6.9%), while RF50r with N = 2200 kN (n = 14.0%). The out-of-plane stability of the walls was ensured by two stiff steel frames with teflon pads placed at the contact points between the frames and the top block. Table 2 summarizes the main properties of the tests.

After the application of the vertical load, N was kept constant, and the walls were loaded with a lateral load at the center of the top concrete block. The load was applied monotonically in four to eight steps until the failure of the specimen. At the end of each load step, a load stage (LS) was performed to mark and measure cracks, as well as to take detailed photographs. The width of the cracks was measured at 21 to 35 locations by using crack comparators.

In addition to crack measurements, the tests also included eight to 12 strain gauges and 22 displacement transducers to obtain continuous measurements of various local and global deformations; refer to Fig. 6. The position of the top block was measured by two horizontal (DT1 and DT2) and two vertical (DT3 and DT4) displacement transducers with respect to the bottom block. For redundancy, the rotation of the top block was also measured with an inclinometer. The strain gauges were attached along the anchorage length of selected longitudinal bars inside the bottom block to measure the pullout of the bars from the block.

TEST RESULTS AND DISCUSSION

Specimen RF30r

To establish a thorough understanding of the behavior of shear-critical walls with UHPFRC jackets, the results from test RF30r are discussed first in some detail. Figure 7 shows the complete shear force versus top displacement response of the specimen. The thick line shows the total displacement measured with displacement transducers DT1 and DT2 (average value), while the thin line represents the displacement resulting only from the opening of the base crack. This latter displacement is equal to the rotation in the base crack times the shear height of the wall a. The rotation in the crack was evaluated by dividing the crack opening measured with

Fig. 5—Test setup.

Table 2—Summary of main test properties

Wall	f_c', MPa	UHPFRC thickness, mm	Surface	Axial load, kN
RF0	52.3	0	—	1200
RF30s	52.6	30	Smooth	1200
RF30r	46.4	30	Rough	1200
RF50r	45.5	50	Rough	2200

DT10 by the distance from the displacement transducer to the neutral axis of the section. The position of the neutral axis as a function of the load was determined from a classical moment-curvature analysis of the base section, where the UHPFRC was taken into account in the compression zone only. This analysis was performed with the measured stress-strain curves of the materials and resulted in the strength prediction shown with a horizontal dashed line in Fig. 7.

In addition to the load-displacement response, the behavior of Specimen RF30r is also discussed with the help of the crack and strain diagrams in Fig. 8. The crack diagrams show the measured crack widths at five load stages (LS1-5), while the strains depict the measurements performed with DT12 and DT13 along the vertical edges of the wall. The photograph in the end of the figure shows the wall after failure.

As evident from Fig. 7, Specimen RF30r behaved linearly up to a load of approximately 200 kN when the base crack (construction joint) began to open, and the stiffness began to decrease very slightly. The construction joint had a negligible tension resistance, but it was initially clamped by the axial load applied on the wall. The non-linearity became much more pronounced when the load exceeded 600 kN and horizontal flexural cracks began to appear above the base crack, refer to LS1 in Fig. 8. As the load increased further, the cracked region extended gradually upwards in the test region, and the cracks began to curve towards the compression toe of the wall due to the effect of shear (flexure-shear cracks, LS2-LS3). By load step LS3 at approximately three-quarters of the peak load V_{max}, the base crack reached a width of 0.4 mm, the steepest flexure-shear crack reached 0.3 mm, and the flexural cracks were in the range of 0.1 to 0.2 mm. It can be seen that the steepest crack was wider

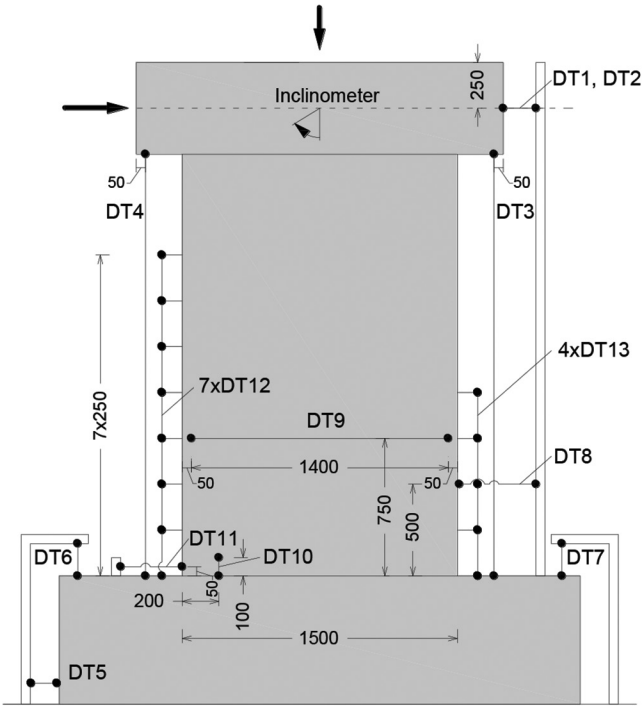

Fig. 6—Instrumentation.

above the UHPFRC jacket than in the region of the jacket. As the cracking progressed, the tangential stiffness of the wall decreased gradually with no sudden increments of the top displacement. By load stage LS4 at 81% of V_{max}, the crack pattern had stabilized, and no major additional cracks formed until failure. Close to this load level, strain gauge measurements showed that the vertical reinforcement began to yield on the tension edge of the base section. This is also evident from the thin line in Fig. 7 that shows the beginning of a fast increase of the rotation in the base section. The last crack measurements were performed at 90% of V_{max} when the base crack and the steepest flexure-shear crack reached widths of 1 and 0.8 mm, respectively. As evident from Fig. 3(b), a crack width of 0.8 mm falls right after the peak response of the steel fibers across the crack. The strains along the tension edge of the wall were highest near the base where the bending moment is maximum (1.65×10^{-3}), but significant strains were also measured higher up the wall above the UHPFRC jacket (0.52×10^{-3}). As the load was finally increased to failure, the load-displacement curve became very flat as a result of the progressive yielding of the layers of the vertical reinforcement in the base section, as well as due to the widening of the major flexure-shear cracks. As evident from Fig. 7, the peak of the curve "touched" the horizontal prediction line, thus confirming that the wall reached its flexural yield capacity. However, soon after the peak point at $V_{max} = 1166$ kN and $\Delta = 28.6$ mm, the displacement capacity of the wall was limited by a sudden shear failure along a diagonal crack (refer to photo in Fig. 8). Twenty-three percent of the displacement capacity Δ_{max} came from the rotation in the base crack, which in turn resulted mainly from the pullout of the vertical reinforcement from the foundation block. No signs of debonding between the concrete and UHPFRC jacket were observed throughout the test.

Effect of UHPFRC jacket and axial force

It is of interest to compare the behavior of Specimen RF30r with a 30 mm thick UHPFRC jacket to that of the reference reinforced concrete Specimen RF0 and the wall with a 50 mm thick jacket RF50r. Figure 9 shows the measured load-displacement response of the three walls. It can be seen that initially the stiffness of the specimens was approximately the same, and that the major flexural cracking in RF0 and RF30r began at approximately the same lateral load of approximately 500 kN. The cracking in RF50r was delayed as this wall was subjected to a higher axial compression load. The equal initial stiffness is consistent with the fact that the UHPFRC had a modulus of elasticity of approximately 30 GPa (Table 1), thus similar to that of normal-strength concrete. However, as the shear was increased above 500 kN, Specimen RF30r exhibited a stiffer response than RF0 due to the more ductile post-cracking behavior of the UHPFRC jacket as compared to the brittle plain concrete. Eventually, the reinforced concrete specimen could not attain its flexural capacity and failed in brittle shear with only minor yielding of the vertical reinforcement near the tension edge of the wall. Therefore, the addition of a 30 mm UHPFRC jacket in RF30r was sufficient to suppress this brittle shear failure and to force a flexural failure of the base section. As a result, Specimen RF30r was 12% stronger than RF0 and had a 30% larger displacement capacity.

Because the 30 mm UHPFRC jacket was sufficient to reach the flexural capacity of the base section, the wall with a 50 mm jacket was loaded with a higher compression load. The goal was to increase the flexural capacity and to study whether the thicker jacket will be sufficient to once again suppress a premature shear failure. As evident from the dashed lines in Fig. 9, the predicted flexural capacity increased by about 20%, and so did the measured strength of RF50r relative to RF30r. The flat plateau of the top curve in the plot shows that the base section of RF50r yielded

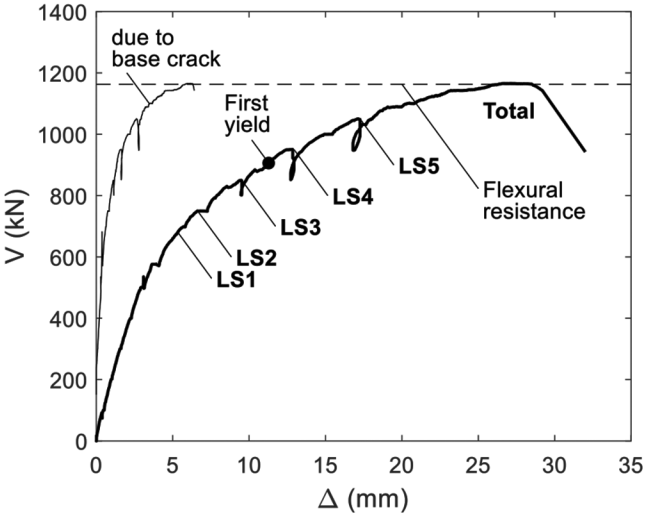

Fig. 7—Load-displacement response of Specimen RF30r.

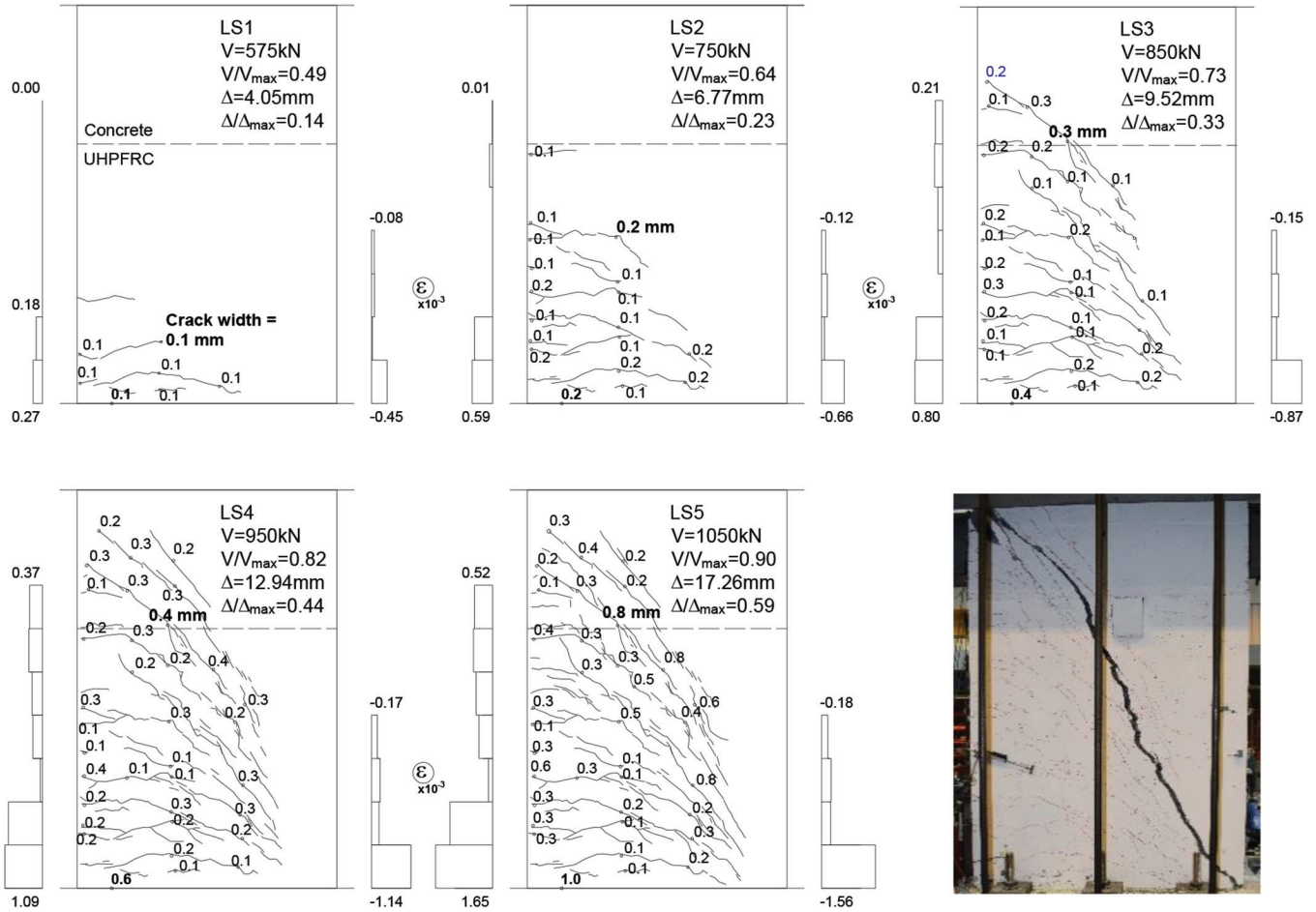

Fig. 8—Behavior of Specimen RF30r.

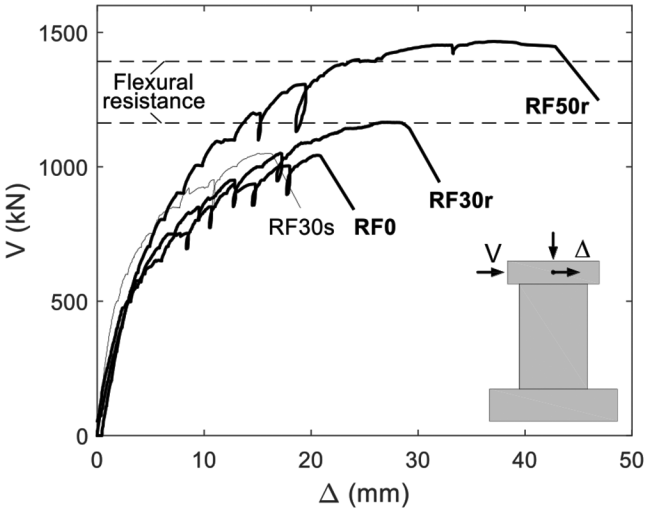

Fig. 9—Load-displacement response of all specimens.

completely in flexure, and the wall exhibited larger ductility than RF30r despite the higher axial load. Nevertheless, similarly to the specimen with a thinner UHPFRC jacket, the displacement capacity of RF50r was eventually limited by a sudden shear failure along a diagonal crack.

In addition to the load-displacement response of the three walls, it is also of interest to compare the crack diagrams of Specimens RF0 and RF30r which had the same axial load. In Fig. 10, the walls are compared at two levels of lateral load: approximately 650 and 950 kN. It can be seen that at the lower load level, due to the high tensile strength of the UHPFRC, the cracking in specimen RF30r had advanced less than that in RF0. While the widest crack in the retrofitted wall was only 0.1 mm, the reference specimen had reached 0.5 mm. At the higher load level, both walls had developed a complete crack pattern; however, the maximum crack widths were again very different: 0.4 and 1.2 mm, respectively. The reason for this difference is mainly the presence of steel fibers in the UHPFRC that bridge the cracks and, together with the reinforcement in the concrete, cause a more dispersed cracking with smaller spacing between the cracks. Therefore, it can be concluded that UHPFRC jackets result in enhanced crack control, and therefore improve the serviceability and durability of retrofitted members.

Finally, as all three walls failed along diagonal cracks, Fig. 11 compares the horizontal expansion of the web of the walls measured with DT9. This expansion can be viewed as the sum of the horizontal displacements in the inclined cracks at 750 mm above the base section, or as the average strain in the stirrups. It can be seen that, due to the high tensile strength of the UHPFRC, the flexural-shear cracks in RF30r began to develop at a higher load than those in RF0. It can also be seen that, for a given load above the cracking load, the web expansion of RF30r was significantly smaller than that of RF0. Nevertheless, as both walls eventually failed in shear along diagonal cracks, they exhibited very similar web expansions at failure. In contrast, Specimen RF50r that failed in a similar manner, developed a significantly smaller ultimate web expansion. This difference will be explained later with the help of a kinematic model of the walls.

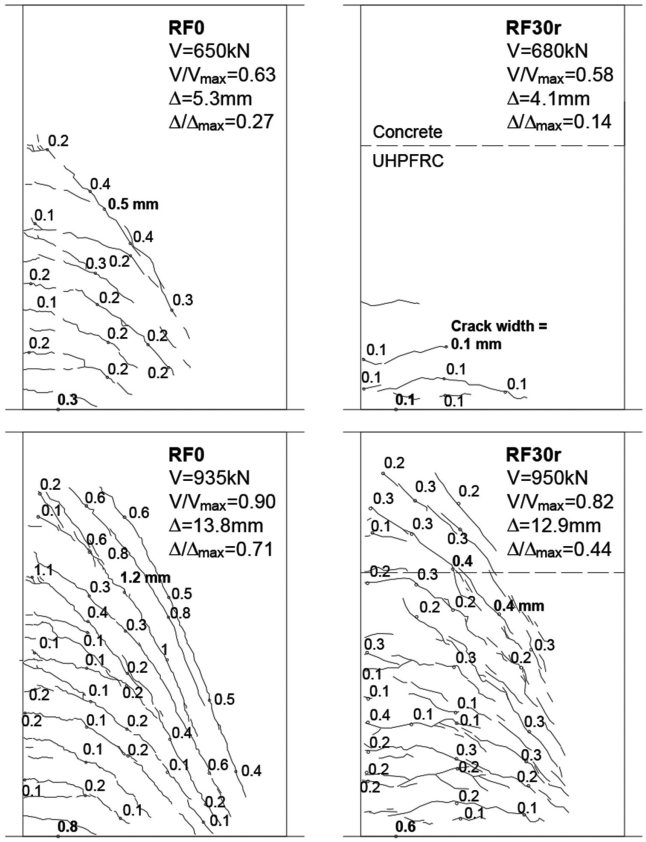

Fig. 10—Crack control provided by UHPFRC jackets.

Effect of concrete surface preparation

Finally, it is of interest to study the effect of concrete surface preparation of existing bridge piers prior to the casting of UHPFRC jackets. In Fig. 9, the load-displacement behavior of Specimen RF30s with a smooth surface (thin line) can be compared to that of RF30r with a rough surface. The two curves are almost overlapping over a large range of the applied load, even though RF30s was slightly stiffer. The stiffer response is explained with the better compacting of the UHPFRC jacket of the wall with a smooth surface. However, as evident from the plot, RF30s failed prematurely at V_{max} = 1050 kN, almost identical to the failure load of the reference specimen without a jacket. Therefore, the UHPFRC jacket of the wall with a smooth surface was ineffective in strengthening the wall.

The reason for this ineffectiveness is illustrated in Fig. 12(a), which compares the crack diagrams of RF30s and RF30r at a lateral load of 950 kN. It can be seen that the cracks in the region of the jacket of RF30s were fewer than those in RF30r, and that the steepest flexural-shear cracks were significantly wider (1.6 mm versus 0.4 mm). The rest of the cracks in the wall with a smooth surface were approximately ~0.1 mm wide, while those in the wall with a rough surface were in the range of 0.1 to 0.4 mm. This shows that, while the deformations in RF30s localized along the diagonal crack, RF30r exhibited much more distributed deformations. As the diagonal crack in RF30s was significantly wider, that caused an early pullout of the steel fibers from the two faces of the crack, and therefore a smaller contribution of the fibers to the shear strength of the wall.

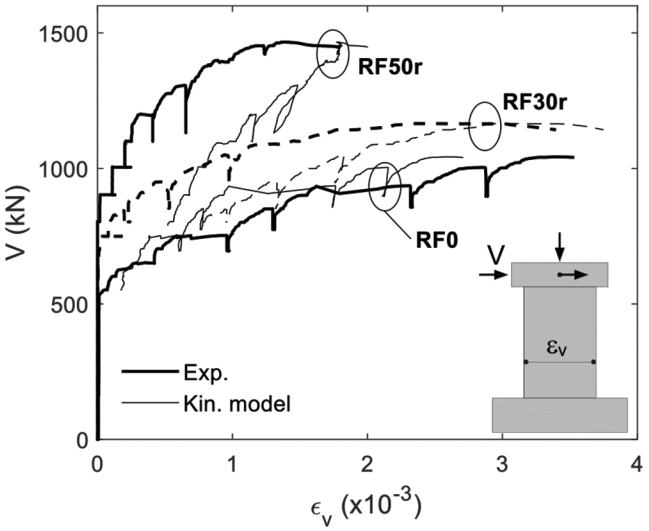

Fig. 11—Effect of UHPFRC jacket on web expansion.

The reason for the crack localization in Specimen RF30s was debonding of the UHPFRC jacket from the concrete. This becomes evident by comparing the cracks above and below the UHPFRC jacket in Fig. 12(a). It can be seen that there is a discontinuity between the two systems of cracks, and therefore the cracks in the jacket did not run through the concrete core. This was confirmed after failure when the slip between the jacket and the concrete core was visible inside the major cracks, refer to the left photo in Fig. 12(b). Therefore, the jacket of Specimen RF30s worked as an external hoop which was separated from the concrete wall but followed the global expansion of the web of the wall. Because the UHPFRC had very limited strain-hardening properties, this global web expansion localized in a single dominant crack in the jacket. Note also that the reinforcing bars were in the concrete core, and thus could not control the cracks in the jacket. As evident from the right-hand photo in Fig. 12(b), debonding was also observed in the compression toe of Specimen RF30s where pieces of the jacket spalled off the wall.

SUMMARY OF TEST RESULTS

Figure 13 shows photographs of the walls after failure and Table 3 summarizes the main test results. It can be seen from the photographs that all four specimens failed along diagonal shear cracks. It can also be seen from the table that the walls with UHPFRC jackets applied on a rough surface were significantly stronger and exhibited a larger displacement capacity Δ_{max} than Specimens RF0 and RF30s, even though their concrete was approximately 13% weaker. Wall RF50r exhibited the largest axial elongation Δ_l and top rotation θ, while RF30s had the smallest values. The sliding displacement Δ_{slip}, measured by displacement transducer DT11 in the base crack (construction joint), was negligibly small for all four walls. The widths of the critical diagonal cracks near failure w_{shear} demonstrate once again the difference in crack control between the walls: the cracks in RF30r and RF50r were two to three times narrower than those in RF0 and RF30s.

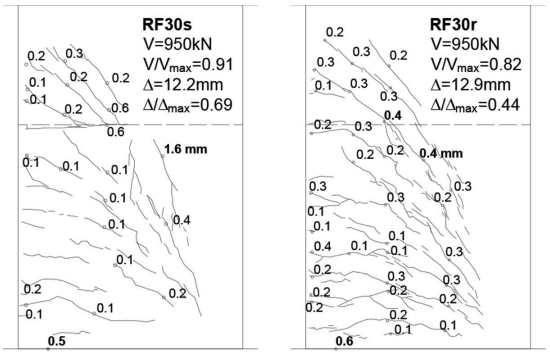

(a) Crack diagrams of RF30s and RF30r at constant lateral load

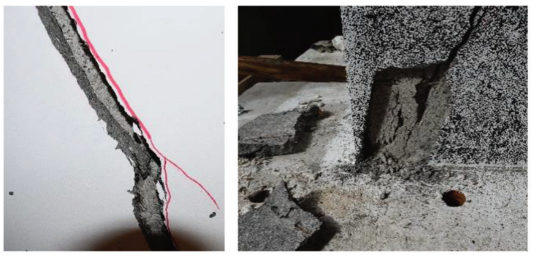

(b) Slip displacement between concrete core and UHPFRC jacket in the critical crack (left) and separation of jacket in compression toe (right)

Fig. 12—Evidence of debonding of UHPFRC jacket.

KINEMATIC ANALYSIS OF WALLS

While the various displacement measurements performed in the tests provide valuable information about the local behavior of the specimens, they do not offer a direct measure of the main deformation modes contributing the global response. In slender walls with aspect ratios a/h larger than approximately 2.5, where the plane sections can be assumed to remain plane, the main deformation modes include flexural curvature and shear strains as defined in the classical beam theory. However, in short walls with $a/h \leq 2.5$ such as the test specimens in this study, plane sections do not remain plane and the deformation patterns differ significantly from those in slender members. To describe these deformation patterns, Mihaylov et al.[23] and Tatar and Mihaylov[24] proposed a three-parameter kinematic theory (3PKT) that uses three degrees of freedom to predict the complete displacement field of diagonally cracked walls. In the following, this model is used to study the deformations of Specimens RF0, RF30r, and RF50r.

Figure 14 shows the three-parameter kinematic model together with a deformation pattern associated with the opening of the base crack. This latter pattern is controlled by the crack width w_b as illustrated in the left-hand diagram in the figure, where w_b results mainly from the pullout of the flexural reinforcement from the foundation block. As a result of the pullout displacements, the wall rotates as a rigid block about the neutral axis of the base section defined by the depth of the compression zone c. This deformation mode was already used to evaluate the thin curve in Fig. 7.

As can be seen from the other three deformation patterns in Fig. 14, the three-parameter kinematic model assumes a straight critical shear crack, as well as a series of radial

Table 3—Summary of test results

Test	f_c', MPa	UHPFRC, mm	Surface	n	V_{max}, kN	Δ_{max}, mm	Δ_l, mm	θ, rad	Δ_{slip}, mm	ε_v, × 10^{-3}	w_b, mm	w_{shear}, mm	V_{max}/V_{flex}
RF0	52.3	0	—	0.066	1043	22.39	3.44	0.0089	0.77	3.53	1.22	1.5	0.95
RF30s	52.6	30	Smooth	0.066	1050	17.7	1.59	0.0063	0.22	3.37	0.86	1.6	0.90
RF30r	46.4	30	Rough	0.075	1166	29.2	2.25	0.0104	0.12	3.40	2.52	0.8	1.00
RF50r	45.5	50	Rough	0.140	1466	42.8	3.89	0.0169	0.87	1.79	5.67	0.5	1.05

Note: f_c' is compressive strength of concrete; $n = N/bh f_c'$ = normalized axial force; N is axial force; b is section width; h is section length; V_{max} is shear force at failure (peak resistance); Δ_{max} is top horizontal displacement at failure; Δ_l is axial elongation = (DT3 + DT4)/2; θ is rotation of top block (inclinometer); Δ_{slip} is slip displacement in base crack = DT11; ε_v is web expansion; w_b is width of base crack; w_{shear} is maximum width of shear cracks at the last load stage prior to failure; V_{flex} is shear corresponding to predicted flexural failure of base section.

Fig. 13—Test specimens after failure.

cracks below the critical crack. These bottom cracks outline a fan of rigid struts centered at the compression toe of the wall and connected to the tension reinforcement (tie). The tie shown in the diagram represents the reinforcement located in the tension half of the section. The concrete above the critical crack is modeled as a rigid block whose position is determined by degrees of freedom (DOFs) $\varepsilon_{t,avg}$, Δ_c, and Δ_{cx}. DOF $\varepsilon_{t,avg}$ is the average strain along the tension reinforcement (tie) and is associated with opening of the fan of struts and rotation of the rigid block about point *A*. DOF Δ_c is the horizontal displacement in the critical loading zone (CLZ) where the concrete crushes at failure, and is associated with a horizontal translation of the rigid block. Finally, DOF Δ_{cx} is the vertical displacement in the CLZ, and is associated with rotation of the rigid block about point *B*.

To determine the values of the four governing kinematic parameters in Fig. 14, it is proposed to use displacement transducers DT3, DT4, DT8, and DT10 (Fig. 6). While parameter w_b is directly equal to the reading of DT10, the three DOFs of the kinematic model $\varepsilon_{t,avg}$, Δ_c, and Δ_{cx} need to be calculated in several steps. First, the readings of DT3, DT4, and DT8 are corrected by subtracting the contribution of the displacements associated with w_b. Second, the corrected vertical displacements DT3* and DT4* are used to interpolate linearly across the width of the top block and to determine the vertical displacements at two locations: the compression edge of the wall and at the location of the vertical tie. The former displacement is equal to DOF Δ_{cx}, while the latter is divided by the cracked length l_t along the tie to determine DOF $\varepsilon_{t,avg}$. The evaluation of l_t is shown in the bottom of Fig. 14. Finally, DOF Δ_c is calculated from

$$\Delta_c = \mathrm{DT8}^* - \left(\frac{\varepsilon_{t,avg} l_t}{d} + \frac{\Delta_{cx}}{d}\right) a_{\mathrm{DT8}} \tag{1}$$

where DT8* is the reading of DT8 corrected by subtracting the contribution of w_b. The expression in the brackets is the rotation of the rigid block due to $\varepsilon_{t,avg}$ and Δ_{cx}, and a_{DT8} = 500 mm is the distance from the base of the wall to DT8.

The results from these calculations for the test specimens at failure are summarized in the table in Fig. 14. In addition to the values of w_b, $\varepsilon_{t,avg}$, Δ_c, and Δ_{cx}, the table also shows their relative contribution to the top lateral displacement Δ_{max} derived from the kinematic model

$$\Delta_{max} = \left(\frac{w_b}{d-c} + \frac{\varepsilon_{t,avg} l_t}{d} + \frac{\Delta_{cx}}{d}\right) a + \Delta_c \tag{2}$$

The expression in the brackets is the rotation of the rigid block, and Δ_c is the horizontal translation of the block. As before, the depth of the compression zone c is evaluated based on the moment-curvature analysis of the base section (refer to values in the bottom of Fig. 14).

It can be seen from Fig. 14 that the base crack w_b and its contribution to Δ_{max} increase with increasing thickness of the UHPFRC jacket. At the same time, reference Specimen RF0 without a jacket exhibited the largest average strain in the fan $\varepsilon_{t,avg}$. This shows that the jackets restrain the opening of the fan and cause localization of plastic strains in the base crack. This is made clearer in Fig. 15, which shows the variation of the strains in the fan at failure measured with displacement transducers DT12. It can be seen that the thicker the jacket, the more localized the strains in the base. The same trend is valid for the compression side of the walls where DOF Δ_{cx} is a measure of the vertical compressive strains in the critical loading zone. As evident from Fig. 14 and 15, the thicker

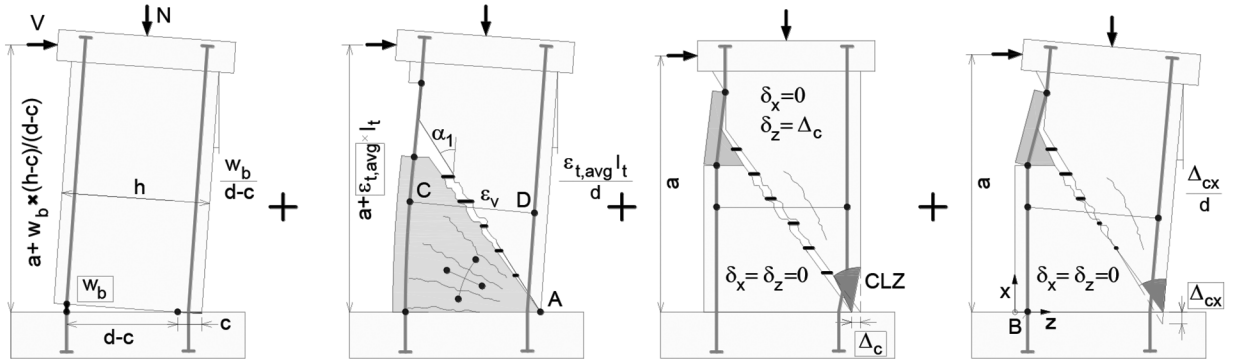

	w_b		$\varepsilon_{t,avg}$		Δ_c		Δ_{cx}	
RF0	1.22 mm	(16%Δ_{max})	3.20×10^{-3}	(59%Δ_{max})	0.65 mm	(3.0%Δ_{max})	2.02 mm	(22%Δ_{max})
RF30r	2.52	(27%)	2.04×10^{-3}	(35%)	2.08	(8.0%)	3.57	(30%)
RF50r	5.67	(39%)	2.72×10^{-3}	(29%)	0.43	(1.0%)	5.12	(31%)

Input geometry: d=1146 mm; h=1500 mm; a=2550 mm
Calculated: c=371 / 297 / 308 mm for RF0 / RF30r / RF50r from-moment-curvature analysis; α_1=33.1°≡angle of wall diagonal α; l_t=d.cot α=1760 mm

Fig. 14—Kinematics of test specimens at failure.

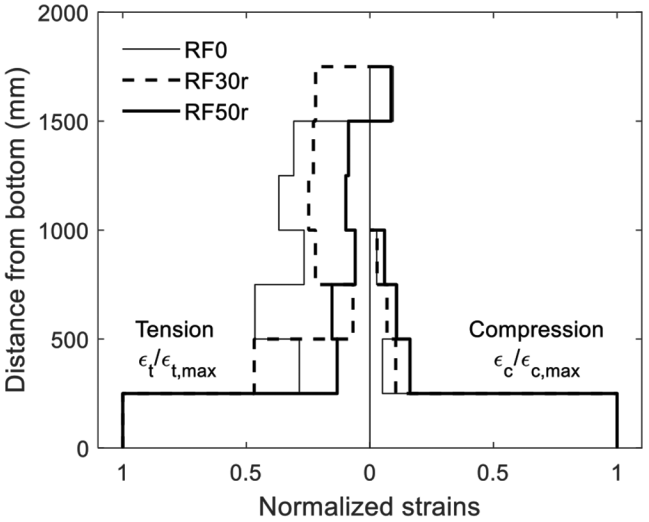

	$\varepsilon_{t,max}$ (x10^{-3})	$\varepsilon_{c,max}$ (x10^{-3})
RF0	11.12	8.56
RF30r	14.40	12.08
RF50r	43.2	17.52

Fig. 15—Variation of strains on flexural-tension and flexural-compression side of test specimens at peak load.

the UHPFRC jacket, the larger the compressive strains and Δ_{cx}. The largest value measured in Specimen RF50r is also a result of the large vertical load applied on this wall. Finally, the most complex trend is observed in the values of DOF Δ_c. The fibers across the critical crack increase the local ductility in shear, and therefore Δ_c tripled from Specimen RF0 to RF30r. However, it appears that the vertical load diminishes Δ_c, and the smallest value of this DOF is recorded in Specimen RF50r.

In terms of contribution to Δ_{max}, it can be seen from Fig. 14 that overall w_b, $\varepsilon_{t,avg}$, and Δ_{cx} are all very significant, while Δ_c contributes with a maximum of 8.0%. Strain $\varepsilon_{t,avg}$ dominates the lateral displacement of Specimen RF0 with 59%, and the trend shifts to w_b as the thickness of the jacket increases. In Specimen RF50r, the contribution of $\varepsilon_{t,avg}$ decreases to 29%, and that of w_b increases from 16% in RF0 to 39%. The intermediate Specimen RF30r features almost equal contributions of w_b, $\varepsilon_{t,avg}$, and Δ_{cx} (~30%). However, it should be noted that in all three walls, the post-peak behavior was dominated by a rapid increase of DOF Δ_c associated with the shear failure. After the tests, the fibers in the UHPFRC jackets were pulled out from the faces of the critical crack in the horizontal direction, and Δ_c measured a few centimeters (refer to Fig. 12(b)).

Finally, it is of interest to verify whether the kinematic model with measured DOFs can predict the expansion of the web of the walls ε_v plotted in Fig. 11. According to the model, ε_v is expressed with $\varepsilon_{t,avg}$, Δ_c, and Δ_{cx} as follows[23]

$$\varepsilon_v = \left(\frac{\varepsilon_{t,avg} l_t}{2d} - \frac{\varepsilon^*_{t,avg}}{4} \right) + \frac{\Delta_{cx}}{2d} + \frac{\Delta_c}{h} \tag{3}$$

where the expression in the brackets is the contribution of the strains ε_t along the vertical tie. The first term in the brackets comes from the horizontal displacement of the compression edge of the wall, and the second term from the horizontal displacement of the tension edge, both evaluated at a height of $h/2$ from the base (refer to points C and D in Fig. 14). Strain $\varepsilon^*_{t,avg}$ is the average strain in the tie within the bottom $h/2$ of the wall evaluated from DT12 minus w_b.

The results from this expression are plotted in Fig. 11 with thin lines. The values of the DOFs were calculated as discussed previously at each load level following the propagation of the major diagonal cracks. By comparing the thin and thick lines of Specimen RF0, it can be seen that the kinematic model with measured DOFs predicts well the measured web expansion along the entire range of ε_v values. For the specimens with jackets, the model overestimates ε_v at low load levels, but gradually approaches the experimental curves and provides accurate predictions prior to

failure. This is because the model assumes a fully cracked member, while the UHPFRC jackets delay the cracking. According to the model, the web expansion of Specimen RF50r was distinctly smaller than those of RF0 and RF30r because of two reasons: the wall with the thickest jacket had the smallest Δ_c and the largest $\varepsilon^*_{t,avg}$ (Eq. (3)).

From this comparison, it can be concluded that the kinematic model, which was originally developed for reinforced concrete walls, can also be used to evaluate the deformations of walls strengthened with UHPFRC jackets. More importantly, as the model captures the web expansion of the wall that governs the shear mechanisms across the critical diagonal cracks, it can be used as a basis of a complete theory to predict the DOFs and entire shear behavior of UHPFRC-strengthened members. This will require an extension of the original 3PKT method that, in addition to kinematics, also includes constitutive relationships and equilibrium conditions.

CONCLUSIONS

This paper presented the results from an experimental campaign on 1500 mm-long reinforced concrete wall-type bridge piers retrofitted with UHPFRC jackets. The variables of the tests were the thickness of the jackets (0, 30, and 50 mm), concrete surface preparation (smooth or rough), and axial load ($n = N/bhf_c' = \sim$6.9% or 14%). The main conclusions of the study are the following:

- Due to the excellent workability of UHPFRC, the study confirmed the feasibility of casting thin and tall layers of this material on very rough concrete surfaces. Simple gravity casting was used to recover the original dimensions of the sections of the walls which had been reduced by water-jetting or negative formwork.
- The specimens with rough water-jetted surfaces showed no debonding of the UHPFRC jacket from the concrete, while the jacket of the specimen with a smooth surface proved to be ineffective due to debonding. Therefore, water-jetting is recommended for the UHPFRC retrofit of existing structures.
- While the reference reinforced concrete specimen failed in brittle shear, the water-jetted walls with 30 and 50 mm jackets reached the flexural capacity of the base section and exhibited enhanced crack control. Therefore, UHPFRC jackets can be used to increase both the shear strength and durability of existing structures.
- Although the retrofitted walls with rough concrete surfaces reached the flexural capacity of the base section, their displacement capacity was limited by sudden opening of diagonal shear cracks. Further experiments are therefore needed to study the effect of UHPFRC jackets with different properties on the ductility of retrofitted walls.
- A three-degree-of-freedom kinematic model was used to deconstruct the deformations of the walls into three distinct modes, plus a rigid-body rotation coming from the opening of the base crack. It was observed that the UHPFRC jackets modify the relative participation of the modes, resulting in larger localization of deformations in the base of the wall.
- It was also shown that, with measured DOFs, the kinematic model can predict accurately the expansion of the web of the walls that controls the shear-resisting mechanisms. Therefore, the model can be used as a basis of a complete theory to predict the DOFs and entire behavior of concrete members strengthened with UHPFRC jackets.

AUTHOR BIOS

Renaud Franssen *is a FRIA (F.R.S.-F.N.R.S.) PhD Student in the Department of ArGEnCo at the University of Liège, Liège, Belgium, where he received his MSc in civil engineering in 2016. His research interests include behavior of ultra-high-performance fiber-reinforced concrete (UHPFRC) and rehabilitation of concrete structures with UHPFRC.*

ACI member **Luc Courard** *is Professor of building materials at the University of Liège. After completing his PhD work on concrete surface characterization in the late 1990s, he went to Laval University, Laval, QC, Canada, for a postdoctoral fellowship devoted to surface preparation of concrete prior to repair. His research interests include concrete surface characterization, new repair materials, and supplementary cementitious materials.*

Boyan I. Mihaylov *is an Assistant Professor of Civil Engineering at the University of Liege. He received his PhD from the University of Pavia, Pavia, Italy, in 2009, and was a Postdoctoral Fellow at the University of Toronto, Toronto, ON, Canada, until 2013. His research interests include the development of his macro-kinematic approaches for the behavior of disturbed concrete regions and members, as well as the assessment and retrofit of existing concrete structures.*

ACKNOWLEDGMENTS

The authors would like to express their gratitude to Service Public de Wallonie for funding the experimental program of this study.

REFERENCES

1. Bruhwiler, E., "Renforcement et Réhabilitation des Structures en Béton au Moyen du BFUP Armé," research seminar at the Université de Liège, Liège, Belgium, 2016.

2. Brühwiler, E., and Denarié, E., "Rehabilitation and Strengthening of Concrete Structures Using Ultra-High Performance Fibre Reinforced Concrete," *Structural Engineering International*, V. 23, No. 4, 2013, pp. 450-457. doi: 10.2749/101686613X13627347100437

3. Charron, J. P.; Denarié, E.; and Brühwiler, E., "Permeability of Ultra-High-Performance Fiber Reinforced Concretes (UHPFRC) Under High Stresses," *Materials and Structures/Materiaux et Constructions*, V. 40, No. 3, 2007, pp. 269-277.

4. Abbas, S.; Nehdi, M. L.; and Saleem, M. A., "Ultra-High Performance Concrete: Mechanical Performance, Durability, Sustainability and Implementation Challenges," *International Journal of Concrete Structures and Materials*, V. 10, No. 3, 2016, pp. 271-295. doi: 10.1007/s40069-016-0157-4

5. Leutbecher, T., and Fehling, E., "Tensile Behavior of Ultra-High-Performance Concrete Reinforced with Reinforcing Bars and Fibers: Minimizing Fiber Content," *ACI Structural Journal*, V. 109, No. 2, Mar.-Apr. 2012, pp. 253-264.

6. Richard, P., and Cheyrezy, M., "Composition of Reactive Powder Concretes," *Cement and Concrete Research*, V. 25, No. 7, 1995, pp. 1501-1511. doi: 10.1016/0008-8846(95)00144-2

7. Noshiravani, T., "Structural Response of R-UHPFRC - RC Composite Members Subjected to Combined Bending and Shear," PhD thesis, École Polytechnique Fédérale de Lausanne, Lausanne, Switzerland, 2012.

8. Sadouki, H.; Bruhwiler, E.; and Zwicky, D., "Chillon Viaduct Deck Slab Strengthening Using Reinforced UHPFRC: Numerical Simulation of Full-Scale Tests," *Proceedings of the 4th International Conference on Concrete Repair, Rehabilitation and Retrofitting,* ICCRRR 2015, 2015.

9. Noshiravani, T., and Brühwiler, E., "Experimental Investigation on Reinforced Ultra-High-Performance Fiber-Reinforced Concrete Composite Beams Subjected to Combined Bending and Shear," *ACI Structural Journal*, V. 110, No. 2, Mar.-Apr. 2013, pp. 251-261.

10. Paschalis, S. A.; Lampropoulos, A. P.; and Tsioulou, O., "Experimental and Numerical Study of the Performance of Ultra High Performance Fiber Reinforced Concrete for the Flexural Strengthening of Full Scale Reinforced Concrete Members," *Construction and Building Materials*, V. 186, 2018, pp. 351-366. doi: 10.1016/j.conbuildmat.2018.07.123

11. Meda, A.; Mostosi, S.; and Riva, P., "Shear Strengthening of Reinforced Concrete Beam with High-Performance Fiber-Reinforced

Cementitious Composite Jacketing," *ACI Structural Journal*, V. 111, No. 5, Sept.-Oct. 2014, pp. 1059-1068. doi: 10.14359/51686807

12. Massicotte, B.; Dagenais, M.-A.; and Lagier, F., "Performance of UHPFR Jackets for the Seismic Strengthening of Bridge Piers," RILEM-*fib*-AFGC International Symposium on Ultra-High Performance Fibre-Reinforced Concrete, UHPFRC 2013, Marseille, France, 2013.

13. Garneau, J.-F., "Réhabilitation Sismique des Piles-Murs de Pont Rectangulaires par Chemisage en Béton Fibré à Ultra-Haute Performance," Université de Montréal, Montréal, QC, Canada, 2015.

14. Beschi, C.; Meda, A.; and Riva, P., "Column and Joint Retrofitting with High Performance Fiber Reinforced Concrete Jacketing," *Journal of Earthquake Engineering*, V. 15, No. 7, 2011, pp. 989-1014. doi: 10.1080/13632469.2011.552167

15. Meda, A.; Mostosi, S.; Rinaldi, Z.; and Riva, P., "Corroded RC Columns Repair and Strengthening with High Performance Fiber Reinforced Concrete Jacket," *Materials and Structures/Materiaux et Constructions*, V. 49, No. 5, 2016, pp. 1967-1978.

16. Adriano, R.; Morbi, A.; and Plizzari, G. A., "Seismic Retrofitting of a Bridge Pier with Ultra High Performance Fibre Reinforced Concrete," *MATEC Web of Conferences*, V. 199, 2018.

17. NF P 18-470, "Ultra-High Performance Fibre-Reinforced Concrete: Specifications, Performance, Production and Conformity," Association Francaise de Normalisation, Paris, France, 2016.

18. NF P 18-710, "National Addition to Eurocode 2: Design of Concrete Structures: Specific Rules for Ultra-High Performance Fibre-Reinforced Concrete (UHPFRC)," Association Francaise de Normalisation, Paris, France, 2016.

19. Choi, M. S.; Kang, S. T.; Lee, B. Y.; Koh, K.-T.; and Ryu, G.-S., "Improvement in Predicting the Post-Cracking Tensile Behavior of Ultra-High Performance Cementitious Composites Based on Fiber Orientation Distribution," *Materials (Basel)*, V. 9, No. 10, 2016, p. 829. doi: 10.3390/ma9100829

20. Wille, K.; Tue, N. V.; and Parra-Montesinos, G. J., "Fiber Distribution and Orientation in UHP-FRC Beams and Their Effect on Backward Analysis," *Materials and Structures/Materiaux et Constructions*, V. 47, No. 11, 2014, pp. 1825-1838.

21. Yoo, D. Y.; Kang, S. T.; and Yoon, Y. S., , "Effect of Fiber Length and Placement Method on Flexural Behavior, Tension-Softening Curve, and Fiber Distribution Characteristics of UHPFRC," *Construction and Building Materials*, V. 64, 2014, pp. 67-81. doi: 10.1016/j.conbuildmat.2014.04.007

22. Maya Duque, L. F., and Graybeal, B. "Fiber Orientation Distribution and Tensile Mechanical Response in UHPFRC," *Materials and Structures/Materiaux et Constructions*, V. 50, No. 1, 2017, pp. 1-17.

23. Mihaylov, B. I.; Hannewald, P.; and Beyer, K., "Three-Parameter Kinematic Theory for Shear-Dominated Reinforced Concrete Walls," *Journal of Structural Engineering*, ASCE, V. 142, No. 7, 2016, pp. 1-14. doi: 10.1061/(ASCE)ST.1943-541X.0001489

24. Tatar, N., and Mihaylov, B., "Kinematic-Based Modeling of Shear-Dominated Concrete Walls with Rectangular and Barbell Sections," *Journal of Earthquake Engineering*, V. 25, No. 7, 2021, pp. 1408-1437. doi: 10.1080/13632469.2019.1577764